Publication Year	2016
Acceptance in OA	2020-05-13T07:47:50Z
Title	The ASTRI SST-2M prototype for the Cherenkov Telescope Array: opto-mechanical performance
Authors	CANESTRARI, Rodolfo, GIRO, Enrico, SIRONI, GIORGIA, ANTOLINI, ELISA, FUGAZZA, Dino Pierluigi, SCUDERI, Salvatore, TOSTI, Gino, Tanci, Claudio, RUSSO, Federico, GARDIOL, Daniele, Fermino, Carlos Eduardo, STRINGHETTI, LUCA, PARESCHI, Giovanni, Marchiori, G., Busatta, A., Marcuzzi, E., Folla, I.
Publisher's version (DOI)	10.1117/12.2232270
Handle	http://hdl.handle.net/20.500.12386/24772
Serie	PROCEEDINGS OF SPIE
Volume	9906

The ASTRI SST-2M prototype for the Cherenkov Telescope Array: opto-mechanical performance

Canestrari, Rodolfo, Giro, Enrico, Sironi, Giorgia, Antolini, Elisa, Fugazza, Dino, et al.

Rodolfo Canestrari, Enrico Giro, Giorgia Sironi, Elisa Antolini, Dino Fugazza, Salvatore Scuderi, Gino Tosti, Claudio Tanci, Federico Russo, Daniele Gardiol, Carlos Eduardo Fermino, Luca Stringhetti, Giovanni Pareschi, G. Marchiori, A. Busatta, E. Marcuzzi, I. Folla, "The ASTRI SST-2M prototype for the Cherenkov Telescope Array: opto-mechanical performance," Proc. SPIE 9906, Ground-based and Airborne Telescopes VI, 990619 (8 August 2016); doi: 10.1117/12.2232270

SPIE.

Event: SPIE Astronomical Telescopes + Instrumentation, 2016, Edinburgh, United Kingdom

The ASTRI SST-2M prototype for the Cherenkov Telescope Array: opto-mechanical performance

Rodolfo Canestrari[*a], Enrico Giro[b], Giorgia Sironi[a], Elisa Antolini[c], Dino Fugazza[a], Salvatore Scuderi[d], Gino Tosti[c], , Claudio Tanci[a], Federico Russo[e], Daniele Gardiol[e], Carlos Eduardo Fermino[f], Luca Stringhetti[g] and Giovanni Pareschi[a], for the ASTRI Collaboration[h] and the CTA Consortium[i] and G. Marchiori[l], A. Busatta[l], E. Marcuzzi[l] and I. Folla[m]

[a] INAF-Osservatorio Astronomico di Brera – Via Bianchi, 46 23807 Merate (Lc) Italy
[b] INAF-Osservatorio Astronomico di Padova – Vicolo Osservatorio, 5 35122 Padova (Pd) Italy
[c] Università di Perugia – Via A. Pascoli 06123 Perugia (Pg) Italy
[d] INAF-Osservatorio Astrofisico di Catania – Via Santa Sofia, 78 95123 Catania (Ct) Italy
[e] INAF-Osservatorio Astrofisico di Torino – Strada Osservatorio 20, 10025, Pino Torinese (To)
[f] Universidade de Sao Paulo Instituto Astronomico e Geofisico – R. do Matao, 1226 Sao Paulo
[g] INAF-Istituto di Astrofisica Spaziale e Fisica Cosmica di Milano – Via Bassini, 15 20133 Milano
[h] http://www.brera.inaf.it/astri/
[i] http://www.cta-observatory.org/
[l] EIE GROUP Srl, via Torino 151A, 30172 Mestre-Venezia
[m] Galbiati Group Srl, Via Cà Bianca Pascolo, 26 - 23848 Oggiono (Lc)

ABSTRACT

ASTRI SST-2M is an end-to-end telescope prototype developed by the Italian National Institute of Astrophysics (INAF) in the framework of the Cherenkov Telescope Array (CTA). The CTA observatory, with a combination of large-, medium-, and small-sized telescopes (LST, MST and SST, respectively), will represent the next generation of imaging atmospheric Cherenkov telescopes. It will explore the very high-energy domain from a few tens of GeV up to few hundreds of TeV.

The ASTRI SST-2M telescope structure and mirrors have been installed at the INAF observing station at Serra La Nave, on Mt. Etna (Sicily, Italy) in September 2014. Its performance verification phase began in autumn 2015. Part of the scheduled activities foresees the study and characterization of the optical and opto-mechanical performance of the telescope prototype.

In this contribution we report the results achieved in terms of kinematic model analysis, mirrors reflectivity evolution, telescopes positioning, flexures and pointing model and the thermal behavior.

Keywords: imaging atmospheric Cherenkov telescope, very high-energy gamma-rays, wide-field aplanatic telescope, CTA, ASTRI, segmented optics

1. INTRODUCTION

Ground-based gamma-ray astronomy has shown that the 10 GeV – 100 TeV energy band can be very powerful to investigate scientific topics where physics is in extreme conditions such as radio-galaxies, pulsars and binary systems, the galactic center, blazars, pulsar wind nebulae and star-forming galaxies. A cost-effective way to perform studies using

[*] rodolfo.canestrari@brera.inaf.it

Ground-based and Airborne Telescopes VI, edited by Helen J. Hall, Roberto Gilmozzi, Heather K. Marshall,
Proc. of SPIE Vol. 9906, 990619 · © 2016 SPIE · CCC code: 0277-786X/16/$18 · doi: 10.1117/12.2232270

this energy band is with ground-based experiments through imaging atmospheric Cherenkov telescopes. Imaging atmospheric Cherenkov telescopes are astronomical instruments that use indirect imaging to detect very high-energy Gamma-ray photons and particles [1]. Gamma-ray photons, ranging from a few GeV up to hundreds of TeV, interacting with the Earth's atmosphere generate an e+e- pair that travels faster than light in the local medium, thus polarizing the nearby molecules. Once these molecules de-excite, a faint flash of beamed visible-near UV photons is emitted (the typical wavelength band is 300-550 nm). This phenomenon is known as the Cherenkov effect [2]. The e+e- pair decays into a lower energy Gamma photon and another positron/electron and so on. This proceeds until the energy of the gamma photons drops below the critical energy for pair production Ec = 83 MeV. Imaging Atmospheric Cherenkov telescopes (IACTs) collect the shower of UV photons generated by Cherenkov effect using suitable multi-pixel sensors, such as photomultiplier tubes. The morphological analysis on the image recorded by the detector returns scientific information on the primary gamma photon, such as the arrival direction and the energy.
The state of the art of such ground-based experiments are H.E.S.S.[3], VERITAS [4] and MAGIC [5]. A breakthrough in this field is expected to happen in the coming years thanks to the Cherenkov Telescope Array (CTA) [6].
The CTA observatory will: increase the sensitivity over currently existing instruments by a factor of 10; expand the detection bandwidth toward the lower and the higher extremes; and improve the angular resolution. This will be possible by the use of cutting-edge technologies and the joint effort of a worldwide consortium of research Institutes and Universities that count about 1200 members within 32 countries. Moreover, CTA will have two observational sites in order to ensure full sky coverage (one for each hemisphere) and it will be composed of telescopes with various sizes. At the southern site, 70 Small Size Telescopes (4 m primary mirror diameter), 25 Medium Size Telescopes (12 m) and 4 Large Size Telescopes (23 m) are envisaged. Additional Schwarzschild-Couder Telescopes (9 m) will be possibly installed to improve the sensitivity at about 1 TeV and to exploit high-precision angular resolution studies. In the northern site, 15 Medium Size Telescopes (12 m) and 4 Large Size Telescopes (23 m) are planned.
Concerning the SST class of telescopes, different options are available for the implementation of the CTA observatory. The Italian National Institute for Astrophysics (INAF) leads one of these; the ASTRI SST-2M is the end-to-end telescope prototype developed in this context. Others options under study can be found in [8] and [9].

The ASTRI SST-2M prototype is the basis of the ASTRI telescopes that will form the mini-array proposed to be installed at the CTA southern site during its pre-production phase. The ASTRI mini-array is a collaborative effort led by INAF along with institutes from Italy, Brazil, and South-Africa. The ASTRI mini-array should then be one of the seed from which the entire CTA southern site will be deployed [10].

In the following sections we give an overview of the opto-mechanical solution and optical layout of the ASTRI SST-2M telescope and then we report some of the results coming out from the on-site optical tests campaign.

2. THE TELESCOPE DESIGN

The mechanical design of the ASTRI SST-2M telescope prototype has been committed by INAF to BCV progetti (www.bcv.it) and Tomelleri (www.tomelleri.com) companies. Details on the design are reported in [11]. The manufacturing of the electro-mechanical structure of the telescope has been awarded to Galbiati group (www.galbiatigroup.it) and EIE group (www.eie.it) companies forming the GEC consortium. Details on the manufacturing are in [12] and [13].
INAF has kept in house the design and the development of optics and mirrors (see [11] and [14]), the detector (see [15], [16] and [17]) and the software (see [18] and [19]).

2.1 The electro-mechanical configuration

The ASTRI SST-2M telescope prototype is shown in Figure 1. The site of installation is the "M. G. Fracastoro" observing station in Serra La Nave (Sicily, Italy), at about 1735 m a.s.l. [20]. It is in operation since September 2014.
This design came about as a trade-off among different configurations to meet the stringent design requirements of the CTA observatory. Finite Elements numerical methods (FE Model and FE Analysis) have been used as design verification tool while on-site tests have been performed to check and validate the models and the analysis. An overview about the results can be found in [13]. Dynamical analyses have also been performed in order to investigate the non-static behavior of the telescope.
The telescope structure is an alt-azimuthal mounting type made of steel grade S355 material. The base is a truncated cone interfaced at the concrete foundation by means of anchor bolts and electrical/communication terminals. A door is

available to give access to these devices. On the top of the base a fork structure makes the connection toward the optical supporting structure. The azimuth bearing, drive system (gear boxes and motors) and encoder are hosted at the interface. The drive system neglects the backlash thanks to two units that work in a master-slave configuration. The fork supports also the electrical cabinets of the telescope. The primary mirror cell, the quadrupod and the secondary mirror back-up structure constitute the optical supporting structure. The cell of the primary mirror is 4.3 meter in side. It hosts 18 reflective segments that compose the entire primary mirror. Each segment can be tip/tilted using a couple of motorized actuators. The secondary mirror is a large monolithic optics supported by a whiffletree system over three actuators. The telescope is moved in elevations by means of a mechanical jack. It is preloaded to reduce the backlash and the telescope is maintained slightly unbalanced about the elevation axis. The fork can rotate around the azimuth axis for 540° while the optical supporting structure can be moved for more the 90° about the elevation axis. The motion control, safety and health monitoring systems are based on PC/PLC solution; the fieldbus is based on EtherCAT standard.

Figure 1: The ASTRI SST-2M telescope prototype installed at the "M. G. Fracastoro" observing station in Serra La Nave (Sicily, Italy) in September 2014.

2.2 The optical layout

IACTs have so far consisted of simple optical configurations with a single reflectior. These solutions provide an almost point-like focus for rays parallel to the optical axis, but suffer from significant aberrations for off-axis rays. Present day IACTs are characterized by angular resolutions on the order of 3-10 arc-minutes over 2°-4° field of view using f/D ranging from 0.7 to 1.2. To significantly enlarge the field of view, an alternative design consisting of a wide field, aplanatic, two-mirror configuration was introduced by Vassiliev et al. [21]. This optical layout is based on the Schwarzschild-Couder solution, initially studied by Schwarzschild in 1905 and later refined by Couder in 1926. This configuration makes use of aspherical reflecting surfaces to correct for spherical and coma aberrations. This asphericity is imparted in the mirrors themselves by means of a suitable manufacturing process. Moreover, the concave secondary mirror is configured to reduce the equivalent focal length in order to enlarge the plate scale. This characteristic is particularly attractive because it opens the almost unexplored possibility to use Silicon photomultipliers sensors. Drawbacks are the large impact angles of the focused rays on the detector surface and the large obstruction of the optical system.

Concerning the solution adopted in the ASTRI SST-2M telescope, it has an equivalent focal length of 2150 mm with an equivalent focal ratio F# of 0.5. The layout is shown in the left panel of Figure 2. It is possible to see the primary mirror composed by 18 segments distributed over 3 rings at different radial distances (green, blue and yellow rings). The focal surface lies upon a convex sphere of 1060 mm in radius of curvature. The 9.6° of corrected field of view are contained within a diameter of only 360 mm with a plate scale of about 37.5 mm/°. The field is sampled with pixels of approximately 0.19°; each one has a square tile shape with pitch of 7 mm. This pixels size guarantees an energy containment of at least the 80% of the entire PSF delivered by the optical system. The trend of the 80% energy containment is shown in the right panel of Figure 2 (this parameter is called D80).

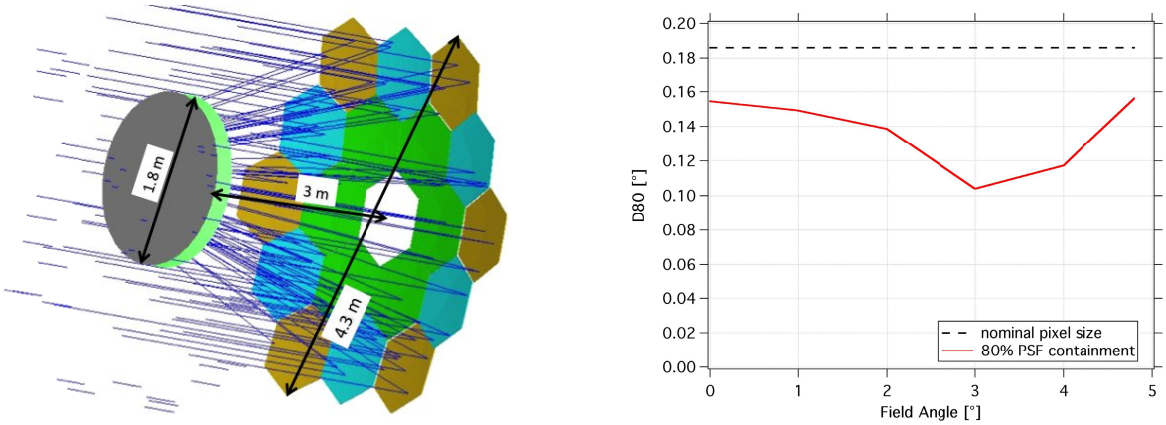

Figure 2: (left) Schwarzschild-Couder layout adopted for the ASTRI SST-2M telescope. The main geometrical distances are also reported. (right) Trend of the 80% energy containment diameter of the point spread function of the optical system implemented of the ASTRI SST-2M telescope prototype.

Concerning the throughput we give in Figure 3 the geometrical area of the ASTRI SST-2M telescope as a function of the field angle, expressed in squared meters. The round markers give the expected area of the system, this values has to be corrected for the actual mirrors reflectivity. It takes into account a number of effects due to the implementation choices or constrains, such as the segmentation of the M1; the detector layout and the vignetting from the structural elements. In particular the diamond markers represent the geometrical contribution of the sole opto-mechanical system.

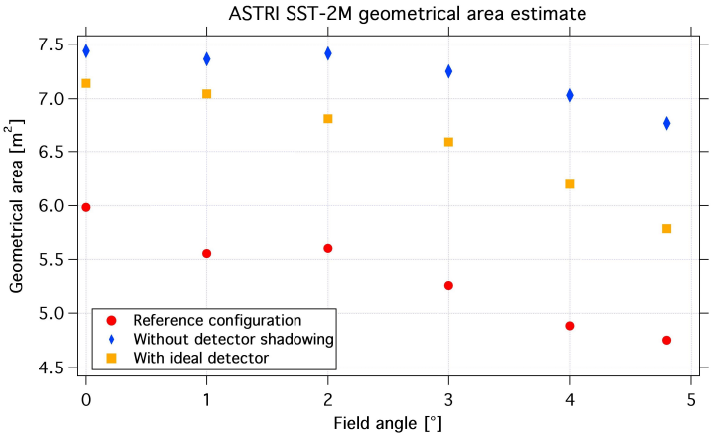

Figure 3: Geometrical area estimate for the optical system (circles) as a function of the field angle and study cases for: absence of the detector (diamonds) and the ideal detector without intra-pixels losses (squares).

Concerning the technologies for the manufacturing of the optical surfaces, for both mirrors we have chosen to adopt the concept of replication. For the primary mirror the technology used is the glass cold shaping process described in [22] and [23]. A glass sheet is bent, at room temperature, by vacuum suction over a replication mold. To keep the shape, a reinforcing core in aluminum honeycomb and a second glass skin are glued together forming a stiff and lightweight sandwich structure. At the end of the polymerization a high reflective coating is deposited on the substrate. This technology, with different implementations, is now being adopted as baseline for manufacturing the entire set of mirrors for CTA. For the secondary mirror, a monolithic glass plate of 19 mm in thickness, we used a thermal bending process developed by the FLABEG company (www.flabeg.com).

3. THE OPTICAL PERFORMANCE

3.1 The kinematic model

The kinematic model is an algorithm able to convert the motor positions of the actuators into the shift of the Point Spread Function onto the focal plane, and vice-versa. The mathematical formulation of this problem can be used mainly for providing a link between the single actuator control and the image shift onto the focal plane. This is also the baseline for the algorithmic coding of the active mirrors control software. For the primary mirror, the kinematic model is expressed by functions (one for each segment) that provide the image position (x, y) onto the focal plane given the step number of the two motors (p, q) of the actuators. In a similar way another function will describe the kinematic model for M2. Once these functions are determined, they can be used both to make predictions and to compute the motor motion needed to generate a desired shift onto the focal plane (by means of the inverse function). From the point of view of the operations the inverse function is the most interesting one because it can be used for this purpose. In our case the explicit form of the direct and inverse functions is not too far from a linear combination of the support position and of the motor position. However, a small non-linearity is present: the first one comes from the eccentricity of the mechanism of the actuators of the primary mirror segments; the second source is given by aberrations introduced by the telescope optics. Regarding the primary mirror, we use a polynomial expansion for the inverse function. To compute the coefficients for each segment a calibration procedure has been put in operation. The parameter space (p, q) is sampled with a given spacing, providing a grid of measured values for (Δx, Δy), thus allowing performing the polynomial fit and computing the coefficients. The results coming from theoretical simulations are presented in Figure 4. Regarding M2 the non-linearity is smaller when compared to the one given by M1 for geometrical reasons and the inverse function can be computed analytically. A detailed description of the kinematic model can be found in [24]. A summary of the mean sensitivities along the two main directions Δx and Δy is reported in Table 1.

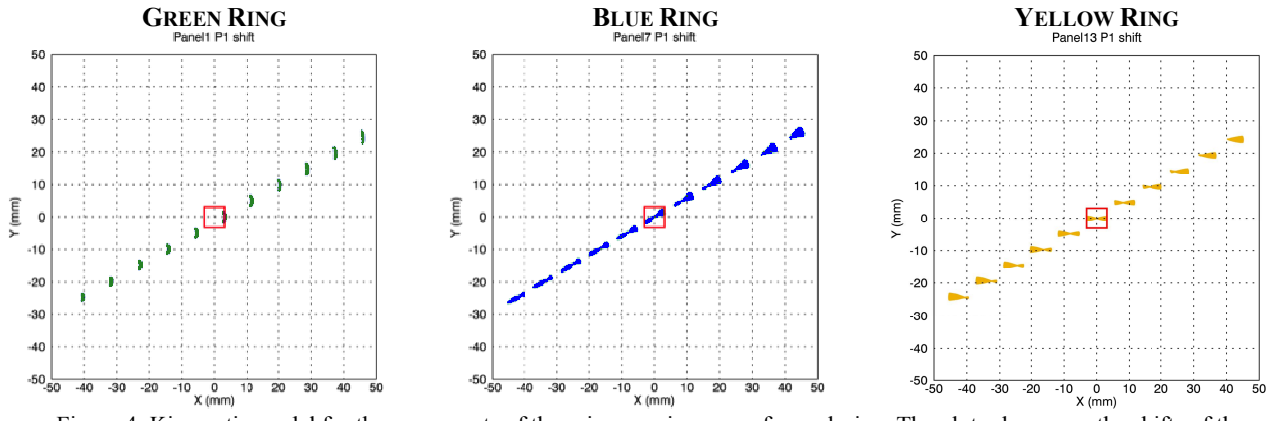

Figure 4: Kinematic model for three segments of the primary mirror, one for each ring. The plots shown are the shifts of the images onto the focal plane as a function of the actuators displacement coming from the simulations.

Table 1 Summary of the mean sensitivity for the primary and the secondary mirrors as resulting from the simulations.

Optical element	**X axis**	**Y axis**
	Expected	Expected
Primary mirror	0.67 arcsec/step	1.16 arcsec/step
Secondary mirror	0.01 arcsec/step	0.14 arcsec/step

3.2 Mirrors reflectivity

The mirror reflectivity measurements have been taken with two different spectrophotometers. The measurements after the manufacturing have been taken using an Ocean Optics device, while all the other measurements taken in situ after the telescope installation have been performed with a Filmetrics device. The Ocean Optics device is the model USB2000+ VIS-NIR equipped with an ISP-REF integrating sphere head. Reflectance measurements have been taken in the spectral range 357-900 nm. Unfortunately, the measurements taken below 470 nm are underestimated because of a strong non-linearity of the detector gain at low photons fluxes. The data have been truncated at 470 nm. The Filmetrics device is the model F20-UVX equipped with an external light source model LS-DT2 (with a Tungsten-Halogen lamp) and a CP-1 contact probe. The CP-1 head is specifically for curved surfaces. Reflectance measurements have been taken in the spectral range 250- 1700 nm.
The surface of each mirror segments of M1 has been sampled with 9 measuring points over 3 diagonals, three points on three diagonals. Concerning M2, the surface is sampled over 4 diagonals. Each diagonal has 9 measuring points. The sampling geometry and positions are shown in Figure 5.

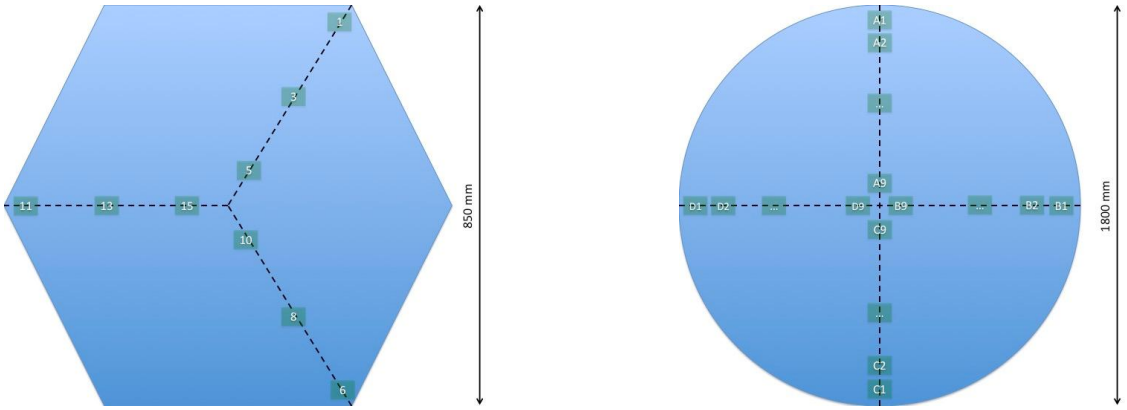

Figure 5: (left) Measuring points on the primary mirror segments. (right) Measuring points on the secondary mirror.

The data are treated as follow. The reflectivity data acquired during the data-taking run (one run corresponds to one mirror for M1) are averaged between those at equal radial distance. Concerning M1, with reference to the left panel of Figure 5, the group of points (1, 6, 11) samples the external part of the mirror, the group (3, 8, 13) samples the middle part and the group (5, 10, 15) samples the inner part of the mirror. The total reflectivity of each mirror is then calculated by weighting the reflectivity of the three groups for the surface area subtended by each one. The external part has a relative weight of 67.3%, the middle part has a weight of 24.5% and the inner part weights for the remaining 8.2%. The total reflectivity of the whole primary mirror of the ASTRI-SST-2M telescope prototype is computed as the average of the 18 mirrors. The data analysis for the secondary mirror undergoes the same mathematical treatment apart from obvious adaptations (number of data points and weights). All the reflectivity data also undergo a chromatic correction to take into account the response of the measuring system (spectrophotometer and optical head) to the wavelengths. This chromatic factor has been obtained thorough the measurement of a calibrated mirror sample done in the laboratory. Moreover, a mirror sample coated with a dielectric multilayer of SiO_2TiO_2 is used to calibrate the maximum reflectivity. In fact the SiO_2TiO_2 sample shows a reflectivity plateau that reach 100%. This has been checked using different

measuring instruments. The stability of the data-taking run is also evaluated. This is done by comparing the curves of the SiO_2TiO_2 sample acquired at the beginning and at the end of the run. Instability up to 2% is tolerated; otherwise the run is repeated.

Regular measuring campaigns have been performed so far. The evolution of the reflectivity for the primary and secondary mirrors is shown respectively in the left and right panels of Figure 6. The ageing effect is noticeably larger than expected from experience with similar coating. This can be attributed to the particularly aggressive environment where the telescope is sited. In fact, the Etna Mount is an active volcano and the eruptions are very frequent making the air locally dense of abrasive and corrosive dust and grains.

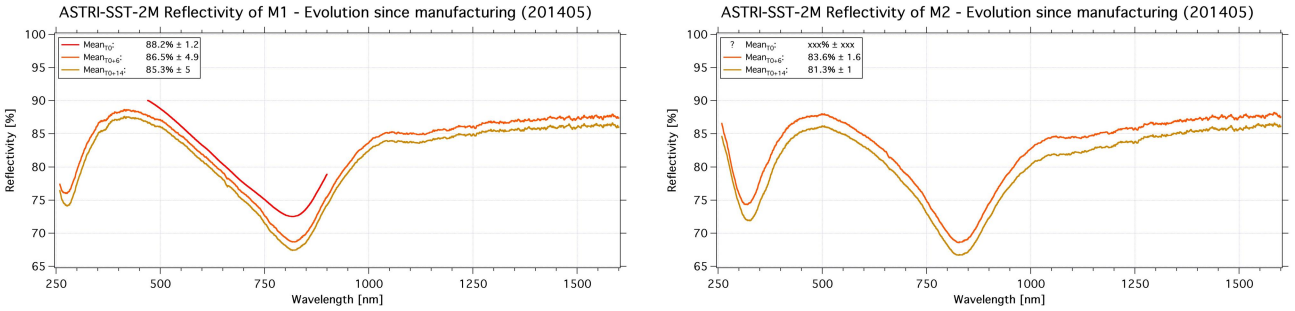

Figure 6: Reflectivity curves measured on the ASTRI SST-2M optics during its lifetime. The values reported for the mean are evaluated in the range 300-550 nm. (left) Primary mirror reflectivity. (right) Secondary mirror reflectivity.

At last, the reflectivity of the entire optical system has been calculated by multiplying the reflectivity of the primary mirror for the reflectivity of the secondary mirror. However, this operation, if applied tout court, introduces an error in the actual reflectivity of the system. This is because all the reflectivity curves shown in this paper are measured with normal incidence while the light rays impinge on the secondary mirror with a mean incident angle of about 46° because of the optical system layout. This effect has been evaluated through simulations and the corrective factor has been implemented. The results are shown in Figure 7.

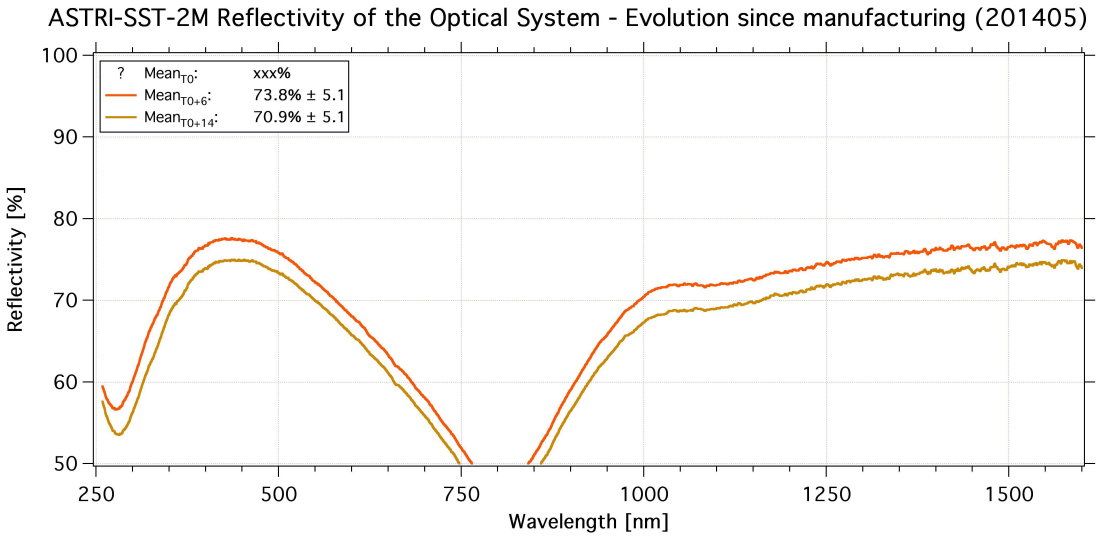

Figure 7: Reflectivity curves for the entire optical system for the ASTRI SST-2M telescope prototype.

4. THE THERMO-MECHANICAL BEHAVIOR

4.1 Thermal stability

Thermal gradients along the telescope structures can affect both the optical quality and the pointing precision of the system by introducing distortion and misalignments between the optical elements. An assessment of these aspects has been performed during the design phase of the telescope. A number of different gradients along the telescopes have been imposed and the resulting effects evaluated. In particular the pointing errors can be very tricky to discover and correct for IACTs. The simulations have shown that gradients on the base along a direction orthogonal to elevation axis as well as along the axis itself can introduce an error up to 4.3 arcsec/°C. In order to verify the real behavior of the telescope we have installed a net of temperature sensors to map the entire system. The sensors are PT100 gauges in a 4-wire connection layout. The topology of the net is shown in Figure 8:

- 4 sensors at the interface between the mast and the M2 back-up structure
- 4 sensors at the interface flange of the focal surface instrument
- 4 sensors at the telescope base
- 4 sensors at the interface between the primary mirror dish and the mast (recently cabled)
- 2 sensors at the elevation axis bearings (recently cabled) + 1 at the elevation jack interface
- 1 sensor on the fork (recently cabled)
- 2 sensors on the counterweights (recently cabled)
- 1 sensor on the secondary mirror (recently cabled)

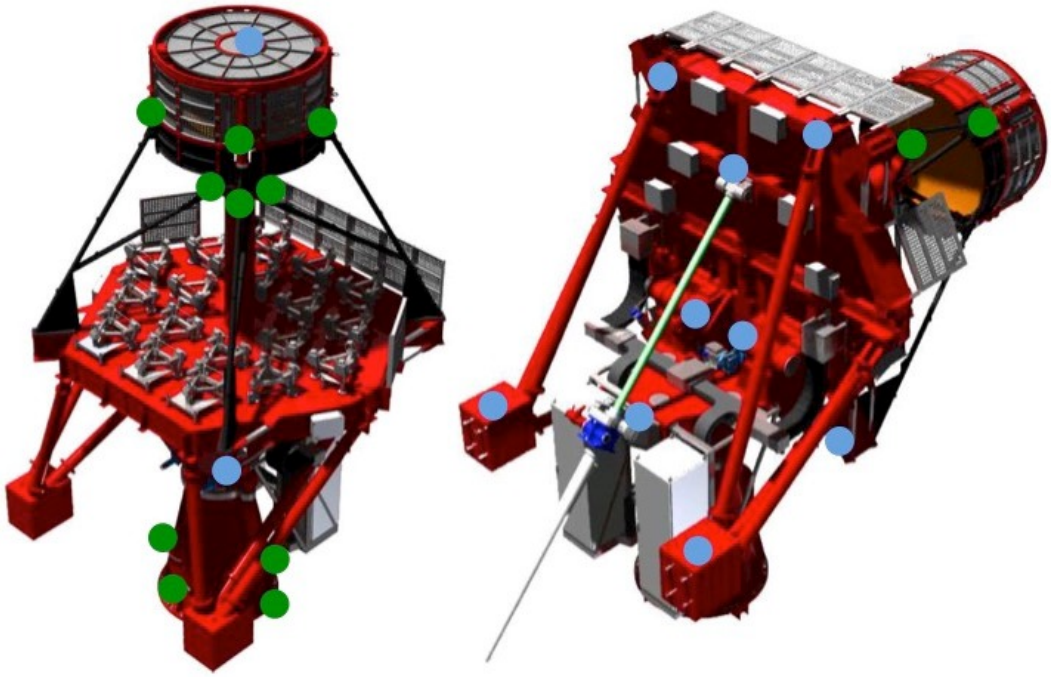

Figure 8: Distributions of the 23 temperature sensors on the ASTRI SST-2M telescope prototype. The green dots represent the sensors in operation since February 2016 while the blue ones have been installed only few weeks ago.

The monitoring of the thermal behavior of the telescope has started in late February and is running almost without uninterruptions since today. Acquisition is made simultaneously on all the sensors with a sampling time of 10 minutes. The recorded data have been analyzed in the topological and time domains.

For the topological domain, in Figure 9 we show the temperature curves during nighttime. Daytime data (based on the astronomical twilight times at the installation site of the telescope) are discarded during the data processing. On each plot we show the temperature distributions along the structures grouped for topological position. In particular we show the behavior of the mast, the camera interface, the base and the dish. In the last plot we summarize the thermal gradients developed on each group: blue, violet green, and red lines for the base, camera, mast and dish respectively. The gradient values within each group are typically below 1.5°C apart from short transients. In particular the base, the most critical telescope part in terms of contributions to the pointing error, is well below 0.5°C for almost all the night times.

Concerning the time domain, the recorded data have also been analyzed to investigate the thermalization capability of the telescope. We look at the temperatures from 3 hours prior the astronomical twilight to 3 hours after it. The telescope follows, with a quite good approximation, the expected exponential decay of the temperatures and at twilight the gradients across the telescope structural components are limited to few degrees. In Figure 10, from left to right, we show: a selected warm night, a selected cold night and the average telescope trends over more than 90 days.

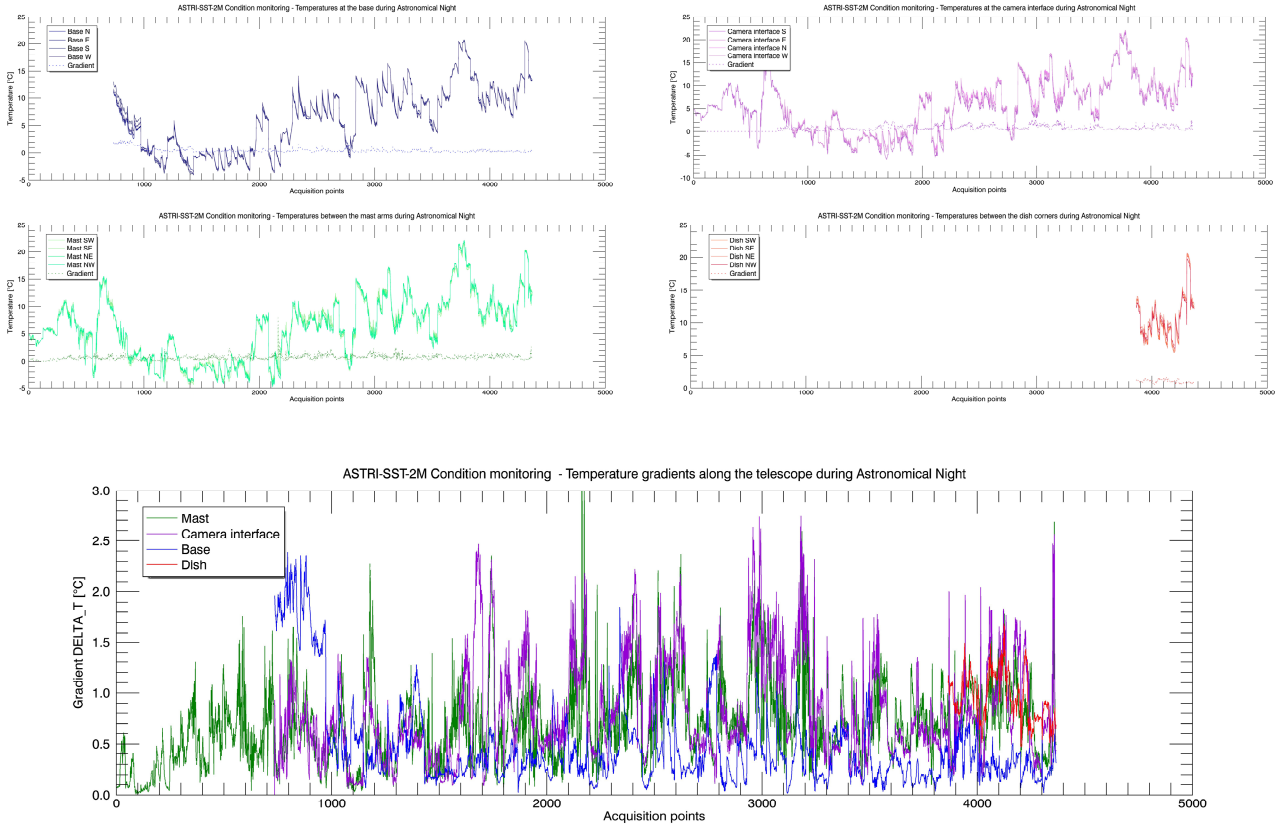

Figure 9: Thermal behavior of the ASTRI SST-2M telescope. The data-points are shown only for the astronomical night timeframe from February to June 2016. (top-left): temperatures at the base, (top-right) temperatures at the interface flange with the focal surface instrument, (center-left) temperatures at the interface between the mast and the secondary mirror supporting structure and (center-right) temperatures at the interface between the mast and the dish. The last graph (bottom) shows the gradients along these structural elements.

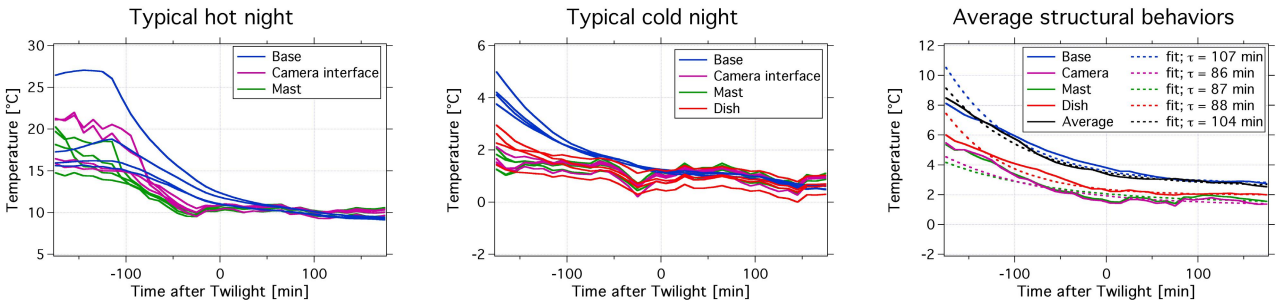

Figure 10: Trends of the ASTRI SST-2M telescope structures in the time domain. The curves show the temperature recorded from 3 hours before the twilight to 3 hours after it. From left to right: a selected warm night, a selected cold night and the average trends for the entire data set. On the right plot, the dashed lines are the exponential fit for each sensors group.

4.2 Positioning, flexures and pointing model

The telescope has been studied also in terms of its pointing characteristics. The flexures of the steel structure and the erection/construction misalignment have been evaluated by means of a series of measurements using sky positions in a similar way used by telescope modeling TPOINT software [26]. Due to the fact the telescope focal plane in normal use could be inaccessible for calibration purposes a tool has been designed and manufactured to obtain the sky position pointing. This is the Pointing Monitor Camera (PMC). The PMC is composed by a CCD camera and a lens. The camera is a Flea3 model FL3-GE-14S3M-C from Point Grey with a detector of 1384x1032 pixels; the optic is a 3 Megapixel lens model H5Z2518C-MO focused at 135 mm. The resulting field of view is of 2.8ºx2.1º with a resolution of about 7.3 arcsec/pixel. The PMC is installed on the back of the secondary mirror support structure. It is coaxial with the telescope opto-mechanical axis within 5 arcmin along the E-W direction (azimuth motion) and within 6 arcmin along the N-S direction (elevation motion). A picture of the PMC installed at the telescope and a bright star used to evaluate its co-alignment with the telescope opto-mechanical axis are shown in Figure 11. Due to its position flexures introducing shift in the telescope focal plane cannot be taken into account in the measurement. However all the other effects (mechanical deviations from design such as non axial perpendicularity) can be estimated.

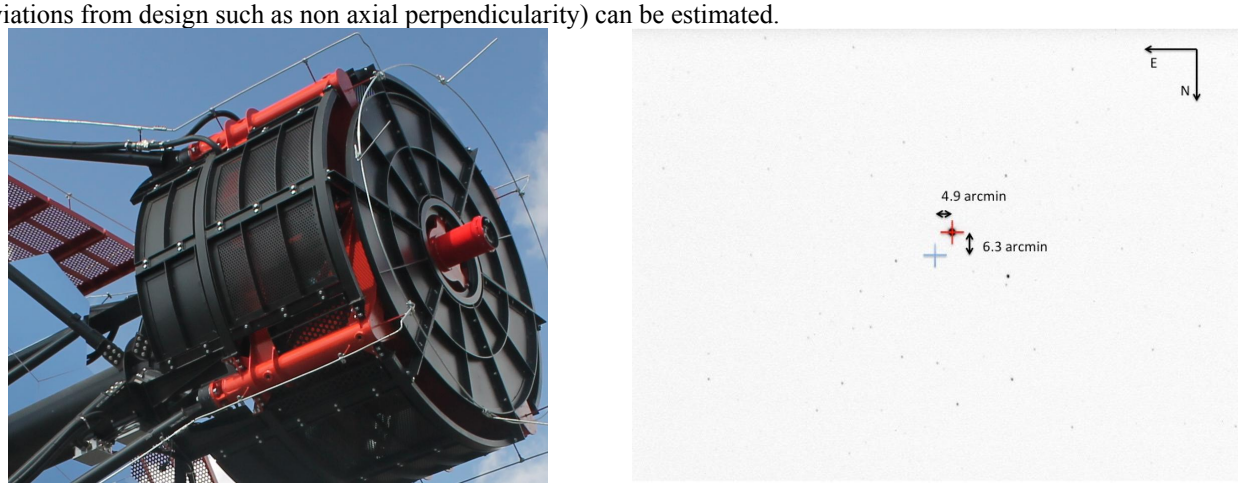

Figure 11: (Left) Picture of the Pointing Monitor Camera installed on the ASTRI SST-2M telescope. (Right) Image taken with the PMC for the evaluation of its misalignment with respect to the opto-mechanical axis of the telescope.

As in the typical telescope pointing model procedures, raw directions of the telescope (elevations and azimuth from encoders readings) are compared with astrometric positions obtained by the PMC. To get these positions the imaged field for each pointing measurement is compared with the asterisms corresponding to that portion of sky in the Tycho-2 [27] and 2MASS [28] catalogues for stars brighter than J equal 9. Using the astrometric coordinates of the stars in the field, it is possible estimate plate scale, distortions, North direction and put them in the form of a SIP (Simple Imaging

Polynomial) solution recorded in the header file of the fits image acquired [29]. To estimate the astrometric accuracy achievable by this procedure a generic field has been acquired with the telescope stopped and the brakes on. A total of 120 images taken every 15 seconds have been obtained. Then the astrometric solution for each frame has been computed and the rms of the center of the field is calculated. The results are reported in Figure 12. The rms error is below 5 arcsec both in RA and DEC coordinates. This value can be considered the best limit that could be achieved by telescope modeling with this method. Due to the fact the specification on telescope pointing is 12 arcsec rms this is fully adequate for our purposes.
Furthermore, this measurement has highlighted an unusual behavior of the elevation axis. The axis shows a very slight movement evaluated in about 16 arcsec/hour even when the control system is completely switched off. The cause of this motion is not yet fully understood and worthy to be further investigated even if this is not affecting in any way on the telescope performance.

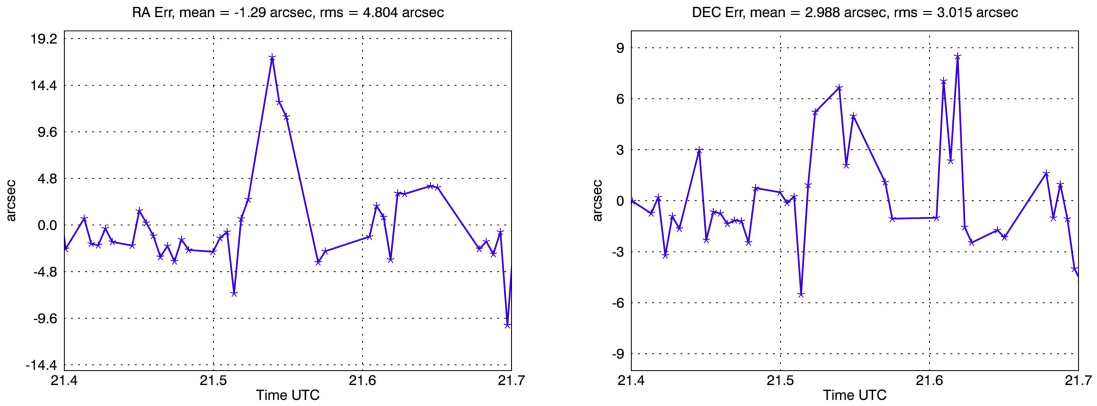

Figure 12: Evaluation of the astrometric accuracy. The rms is below 5 arcsec for both RA and DEC coordinates

The flexures of the optical supporting structure have been measured from a repetition of elevation pointing. For a chosen azimuthal position the telescope has been pointed from 20º above the horizon up to 80º, with steps of 10º. For each position an image of the sky has been acquired by the PMC. The astrometric solution has been used to evaluate the coordinates of the pointing. The optical supporting structure turns to be very stiff. The flexures show a peak-to-valley error of about 65 arcsec on the full range with a better performance for elevation angles from 20º to 70º. This measurement has been repeated to highlight any hysteresis behavior. In fact some hysteresis is present with amplitude of about 10 arcsec. These values are within the specification of the telescope. The results are shown in Figure 13.

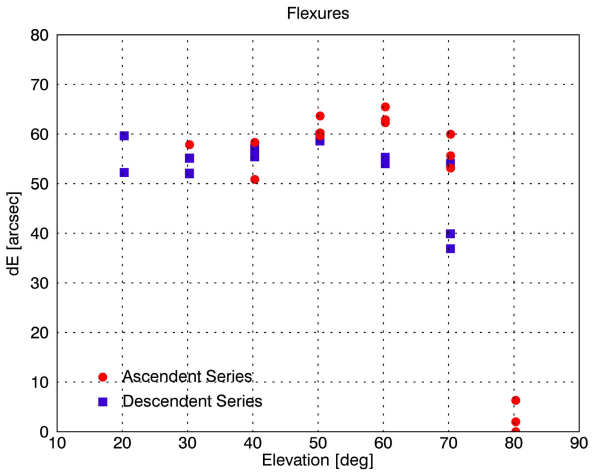

Figure 13: Flexures measured for a chosen azimuthal position for elevation angles between 20º and 80º.

A comprehensive pointing session has been also conducted to derive the full set of positioning errors of the telescope system. Following TPOINT philosophy, an IDL (Interactive Data Language) fitting program has been written to find the best solution as function of these telescope parameters:

Table 2: TPOINT parameters used for fitting the telescope model.

Parameter TPOINT code	***Parameter***	***TPOINT Formula***	***Fitted value (arcsec)***
IA	Index error in azimuth		-1861
IE	Index error in elevation		-533
NPAE	Az/El non-perpendicularity	ΔA= NPAE * tan E	-30
CA	Non-perpendicularity of elevation and pointing axes	ΔA = CA * sec E	-222
AN	North-South misalignment of azimuth axis	ΔA = AN * sin A * tan E ΔE = AN * cos A	-22
AW	East-West misalignment of azimuth axis	ΔA = − AW * cos A * tan E ΔE = AW * sin A	2821
TF	Tube flexure sin E law	ΔE = − TF * cos E	38

Fitted data are obtained using a full azimuthal range mapped with steps of 15º; for each position seven acquisitions at different elevation angles are taken. A second independent set of data for each azimuthal position and the seven elevation values has been obtained to have a cross check of the model. Sky errors result below 10 arcsec rms (against 12 arcsec required) confirming the suitability of ASTRI telescope design.

Only two terms are above what we expected by simulations. CA parameter is about 4 arcmin and AW is above 0.7 deg. In both cases the reason is easily found. CA parameter can be explained considering that there is an intrinsic alignment error of the PMC due to its mechanical holder on the telescope. The quite high CA value takes into account for this.

AW shows an important tilt of the azimuth axis along the E-W direction. Since this tilt has been measured by mechanical methods during the telescope erection to be within 20 arcsec, this deviation can be ascribed to a structural adjustment of the foundations. In fact the soil where the telescope is installed is not particularly stiff and the reinforced concrete slab is supported by micro-poles to go to the proper depth where the rocks are stiffer. Anyway, due to the large variation occurred this tilt should be monitored.

Other sources of errors such as the tilt of the azimuth axis on the N-S direction, non-perpendicularity of the azimuth/elevation axes and flexures are limited to few tens of arcsec. The overall set of measure has been repeated to check the consistency of the results. In Figure 14 and Figure **15** graphical estimations of the errors is shown. In both the plots the main contribution due to the tilt of azimuth axis is dominant. Despite of that the model can recover most of the errors performing inside specifications.

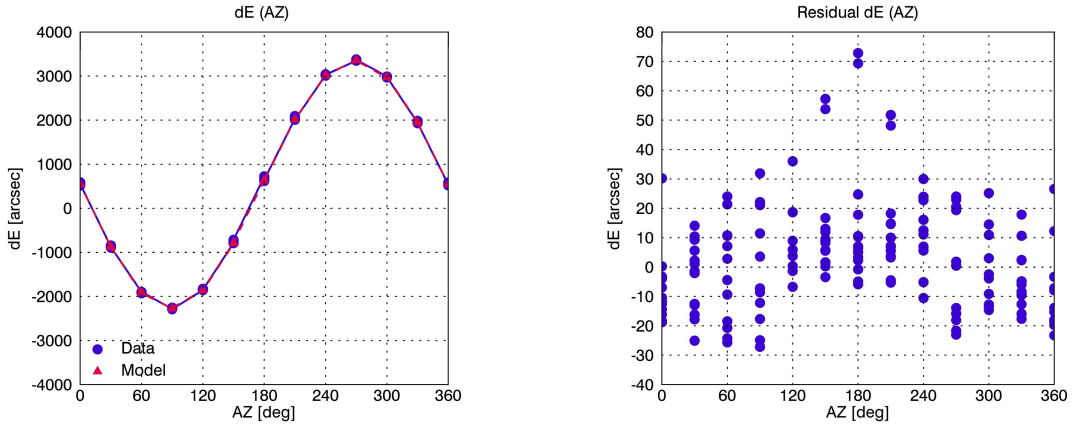

Figure 14: Error in elevation and its fit (left), residual after the model (right). The quite important azimuth tilt is evident in the left panel

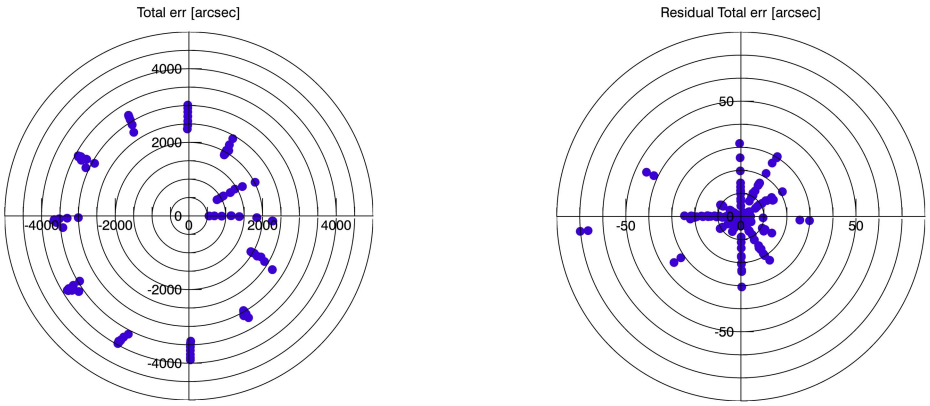

Figure 15: Total error on the sky before model (left) and after the fit (right). The quite important azimuth tilt is evident in the left panel.

5. CONCLUSIONS

This paper presents the in-situ measurements of the ASTRI SST-2M telescope prototype concerning some of the aspects related to the optical and opto-mechanical performance. In particular we are studying the thermal behavior of the mechanical structure. A network of 23 sensors is continuously monitoring the telescope and some insight on the thermal stability of the telescope is already available. Even if a larger data set is needed for completing the investigation, from the data acquired so far it is possible to access the thermal trend of the telescope. Temperature gradients are quite limited along the structure and the ability of the structural elements to reach equilibrium is considered satisfactory. Other aspects being investigated are related to the flexures of the optical supporting structure and the positioning errors of the electro-mechanical system. Apart from a large tilt of the azimuth axis with respect to the gravitational vector, the performance are considered very good. Residual errors are limited to about 10 arcsec and the hysteresis is minimal.
Concerning the optical aspects, the reflectivity of the system is being monitored with regularity since the mirrors manufacturing. An accelerated degradation is recorded with respect to past experiences observed by the authors. However, it has to be mentioned that the installation site of the ASTRI SST-2M telescope is on the slopes of an active volcano where the frequent eruptions make the atmosphere more aggressive in terms of mechanical and chemical actions.
Further studies concerning the behavior of the optical performance for on-axis and off-axis sources are scheduled for the next months.

ACKNOWLEDGMENTS

This work is supported by the Italian Ministry of Education, University, and Research (MIUR) with funds specifically assigned to the Italian National Institute of Astrophysics (INAF) for the Cherenkov Telescope Array (CTA), and by the Italian Ministry of Economic Development (MISE) within the "Astronomia Industriale" program. We acknowledge support from the Brazilian Funding Agency FAPESP (Grant 2013/10559-5) and from the South African Department of Science and Technology through Funding Agreement 0227/2014 for the South African Gamma-Ray Astronomy Programme. We gratefully acknowledge support from the agencies and organizations listed under Funding Agencies at this website: http://www.cta-observatory.org/.

REFERENCES

[1] Galbraith, W. and Jelly, J. V., "Light Pulses from the Night Sky associated with Cosmic Rays," Nature 171, 4347 (1953)
[2] Cherenkov, P. A., "Visible Radiation Produced by Electrons Moving in a Medium with Velocities Exceeding that of Light," Phys. Rev. 52, 378-379 (1937)
[3] Hoffmann, W., et al., "The high energy stereoscopic system (HESS) project," Contribution to AIP 515, 1999
[4] Holder, J., et al., "Status of the VERITAS Observatory," Contribution to AIP 1085, 2008
[5] Ferenc, D., et al., "The MAGIC gamma-ray observatory," NIM-A 553, 274-281, 2005
[6] Acharya, B. S., et al., "Introducing the CTA concept," Astroparticle Physics 43, 3-18, 2013
[7] Oakes L., et al., "Results and developments from the 12m Davies-Cotton MST prototype for CTA," Proceeding SPIE 9603, 960305 (2015)
[8] Dournaux, J. L., et al., "GCT, an end-to end SC telescope prototype for the CTA", this conference (2016)
[9] Schioppa, E. J., et al., "The Single Mirror Small Size Telescope (SST-1M) of the Cherenkov Telescope Array", this conference (2016)
[10] Pareschi, G., et al., "The ASTRI SST-2M prototype and mini-array for the Cherenkov Telescope Array (CTA)", this conference (2016)
[11] Canestrari R., et al., "The ASTRI SST-2M prototype for the next generation of Cherenkov telescopes: structure and mirrors," Proceeding SPIE 8861, 886102 (2013)
[12] Marchiori G., et al., "The ASTRI SST-2M prototype for the next generation of Cherenkov Telescope Array: prototype technologies, goals, and strategies for the future SST," Proceeding SPIE 9145, 91450L (2014)
[13] Canestrari R., et al., "The ASTRI SST-2M prototype for the Cherenkov Telescope Array: manufacturing of the structure and the mirrors," Proceeding SPIE 9145, 91450M (2014)
[14] Rodeghiero, G., at al., "Qualification and testing of a large hot slumped secondary mirror for Schwarszchild-Couder Imaging Air Cherenkov Telescopes," PASP, (2016)
[15] Catalano O., et al., "The camera of the ASTRI SST-2M prototype for the Cherenkov Telescope Array," Proceeding SPIE 9147, 91470D (2014)
[16] Sottile, G., et al., "ASTRI camera electronics", this conference (2016)
[17] Impiombato, D., et al., "Temperature characterization of the CITIROC front-end chip", this conference (2016)
[18] Tosti, G., et al., "The ASTRI/CTA mini-array software system," Proceeding SPIE 9152, 915204 (2014)
[19] Tanci, C., et al., "The ASTRI Mini Array Software System (MASS) implementation: a proposal for the Cherenkov Telescope Array", this conference (2016)
[20] Maccarone, M.C., et al., "The Site of the ASTRI SST-2M Telescope Prototype," Proceeding 33rd ICRC 0110, (2013)
[21] Vassiliev V., Fegan S. and Brousseau P., "Wide field aplanatic two-mirror telescopes for ground-based γ-ray astronomy," Astroparticle Physics 28, 10-27 (2007)
[22] Canestrari R., et al., "Cold-shaping of thin glass foils as novel method for mirrors processing. From the basic concepts to mass production of mirrors," Optical Engineering 52, 051204-1 (2013)
[23] Canestrari R., et al., "An overview on mirrors for Cherenkov telescopes manufactured by glass cold-shaping technology," Proceeding SPIE 9603, (2015)
[24] Gardiol, D., et al., "Active Optics system of the ASTRI SST-2M prototype for the Cherenkov Telescope Array," Proceeding SPIE 9151, 915103 (2014)
[25] Sironi G., et al., "ASTRI SST-2M Cherenkov Telescope Array prototype: M1 characterization," Proceeding SPIE 9603, 960303 (2015)
[26] Wallace, P. T., "TPOINT -- Telescope Pointing Analysis System," Starlink User Note 100, (1994)
[27] Høg E., et al, "The Tycho-2 Catalogue of the 2.5 million brightest stars," Astron. Astrophys. 355, 27–30 (2000)
[28] Jarrett T. H, et al, "2MASS extended source catalog: overview and algorithms," The Astronomical Journal 119, 2498 (2000)
[29] Shupe, D. L.; et al., "The SIP Convention for Representing Distortion in FITS Image Headers," Astronomical Data Analysis Software and Systems XIV ASP Conference Series 347, 491 (2005)